Simulation of thermal field distribution in biological tissue and cell culture media irradiated with infrared wavelengths

VIKTOR DREMIN,[1,2,*] **ID IRINA NOVIKOVA,**[2] **AND EDIK RAFAILOV**[1]

[1]*College of Engineering and Physical Sciences, Aston University, Birmingham, B4 7ET, UK*
[2]*Cell Physiology and Pathology Laboratory, Orel State University, Orel, 302026, Russia*
[*]v.dremin1@aston.ac.uk

Abstract: In recent years, there has been a growing interest in the singlet form of oxygen as a regulator of the physiological functions of cells. One of the ways to generate singlet oxygen is direct optical excitation of the triplet oxygen form. Since molecular oxygen weakly absorbs light, high power is required to obtain sufficient concentrations of singlet oxygen. However, the increase in the radiation power of laser can induce a local temperature increase around the laser spot. This may be critical considering the temperature governs every biological reaction within living cells, in particular. Here, the interaction of laser radiation of infrared wavelengths, generating singlet oxygen, with biological tissues and cell culture media was simulated. Using the COMSOL Multiphysics software, the thermal field distribution in the volume of skin, brain tissue and cell culture media was obtained depending on the wavelength, power and exposure time. The results demonstrate the importance of taking temperature into account when conducting experimental studies at the cellular and organismal levels.

1. Introduction

Oxygen and its partially reduced chemical products, known as reactive oxygen species (ROS), have important regulatory and signaling functions [1,2]. Oxygen is an electron acceptor in the mitochondrial respiratory chain and a substrate for enzymes that catalyze oxidase and oxygenase reactions, but on the other hand, the mitochondrial electron transport chain is a source of potentially dangerous and toxic ROS [3]. The experience gained from studying the physiological and pathological role of ROS and the mechanisms of their generation has provoked interest in a singlet form of oxygen ($^1O_2$).

Singlet oxygen $^1O_2$ is a common name for the electronically excited state of triplet oxygen. The $^1O_2$ oxygen is formed when the spin of one of the electrons located on different π-antibonding orbitals of the oxygen molecule changes. Molecular oxygen has two low-lying singlet excited states above the triplet state. These states differ, in addition to differences in electronic configurations, in energy and lifetime. The reactivity of the excited state is several orders of magnitude greater than that of the triplet form of oxygen, which, due to its biradical chemical character, is unreactive to most chemical compounds [4]. The $^1O_2$ oxygen exhibits considerable reactivity toward electron-rich organic compounds, especially, lipids, proteins, nucleic acids and ribonucleic acid [1,5,6]. This leads to the formation of such reactive substances as endoperoxides, radicals, ROS, peroxides, aldehydes, etc.

The appearance of data on the participation of singlet oxygen in the regulation of physiological functions of cells and the possibility of its activation with the use of photosensitizers have made a significant step towards understanding the role of this highly reactive type of oxygen as the main mediator of therapeutic effects in photodynamic therapy (PDT) [7,8]. Photosensitized generation of $^1O_2$ requires only oxygen, light of an appropriate wavelength, and a photosensitizer capable of absorbing and using that energy to excite oxygen to its singlet state (see left side of Fig. 1) [9].

The $^1O_2$ oxygen is produced via energy transfer during the collision of an excited sensitizer with triplet oxygen. The excitation of the sensitizer is usually achieved by using a one-photon transition between the ground state (PS_0) and the singlet excited state ($^1PS^*$) after light illumination in the of visible or NIR spectral range. Intersystem crossing generates the triplet state of the sensitizer ($^3PS^*$) with a longer lifetime than that of $^1PS^*$. In the $^3PS^*$ state, the sensitizer reacts with the oxygen molecule. Sensitizers can accumulate in various cell compartments (for example, mitochondria, lysosomes, endoplasmic reticulum, Golgi apparatus) [10]. So the effectiveness of PDT varies depending on the characteristics of selective accumulation of a sensitizer in target tissues.
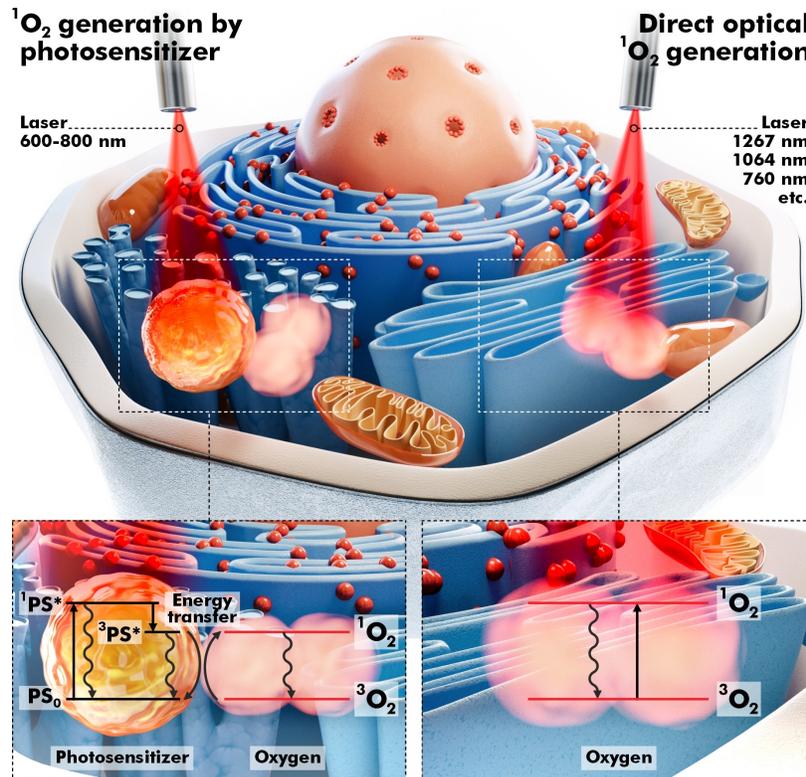
Fig. 1. Two main mechanisms of $^1O_2$ generation. Left side – photodynamic mechanism of $^1O_2$ generation by photosensitizer through energy transfer to oxygen from singlet and triplet exited states of photosensitizer ($^1PS^*$ and $^3PS^*$) and right side – direct optical generation of $^1O_2$. 1267, 1064 and 760 nm are the maxima of light absorption by molecular oxygen.

The possibility of direct excitation of an oxygen molecule by light in the ground triplet state and regulation of its production by changing the light intensity and exposure time is of undoubted interest for fundamental and practical medicine. The basic triplet state of oxygen has several absorption bands in the infrared and visible regions (optical range between 1300 nm and 390 nm), at which singlet oxygen can be produced (see right side of Fig. 1) [11]. Photon absorption in the particular absorption wavelengths corresponding to different electronic-vibrational molecular levels leads to the excitation of the specific $^1O_2$ state. A single photon can generate one or two $^1O_2$ molecules, and thus the monomol and dimol transitions are realized. The 1267 nm, 1064 nm and 760 nm bands are most widely used to directly generate $^1O_2$ [12–15]. In [16], some other light wavelengths are applied to excite oxygen molecules.

Recent studies on direct excitation of oxygen have provided results that describe laser initiation of oxidative stress, destabilization of cell metabolism after the end of the effect [17], induction of tumor cell death [18], and a relationship between the dose of laser exposure and cell death [19]. It was found that the generation of singlet oxygen induced by different doses of laser radiation can also act as an activator of mitochondrial respiration and ATP production in the brain [20].

Despite the growing interest in the method of direct generation of $^1O_2$, it has one serious disadvantage (poor light absorption of molecular oxygen), which can be compensated by changes in light intensity and exposure time [16]. However the increase in the radiation power of laser can induce a local temperature increase around the laser spot [21]. Although absorption by H_2O is relatively low below 1300 nm and significantly decreases in the region of spectrum from 950 nm and below [22], the increase in radiation power and heat transfer to the immediate environment could produce small but significant local thermal effects around the laser spot [21]. This may be critical considering the temperature governs every biological reaction within living cells, in particular, the temperature increase can possibly induce cytotoxic effects or cell death.

Currently, various approaches are used to control the intracellular heating level. For instance, [21] determined that a simple thermal sensor may disrupt the system, and thus it cannot be used for temperature measurements. In addition, the use of remote thermal imaging does not allow to obtain a temperature distribution over the depth of living tissue. Fluorescent dyes Rhodamine B and Rhodamine 110 whose fluorescence intensities are characterized by different temperature dependence demonstrated the possibility of controlling the temperature [23–25]. Control of temperature changes can also be carried out by analyzing the fluorescence emission shifts of another temperature-sensitive dye probe of Laurdan [26]. In [27,28], fluorescent polymers and fluorescent proteins were suggested to use for temperature mapping within a living cell. However, these approaches have some disadvantages such as low sensitivity and systematic errors due to fluctuations in the fluorescence rate and the influence of the optical properties of the environment [27,29]. Another limitation of these approaches is that they need preincubation ("loading") of cells with dyes for *in vivo* studies.

Modern computer modeling makes it possible to describe various physical processes with high accuracy, including the propagation of optical radiation in media. In this paper, we present one of such approaches to the description of heating in the media caused by exposure to laser radiation.

The purpose of this study is to find the optimal ratio of laser radiation parameters and exposure time for further investigation of the effects of singlet oxygen. To this end, *in silico* studies were performed to investigate how the optical radiation of various wavelengths for direct optical generation of singlet oxygen interacts with biological tissues and to model the resulting thermal effects. The cell culture media (CCM) in a coverslip cell chamber, the brain tissues and the skin were viewed as objects of research. This choice is due to the fact that various cell lines from melanoma cells to neurons are the most studied object of the influence of singlet oxygen. The brain is also actively explored in various applications of PDT, optical stimulation and optogenetics. The high frequency of detection of skin cancer relative to other types of cancer, the availability of the treatment area, as well as the possibility of instrumental control of the effectiveness of the therapy also determines the prospects of using direct optical generation of singlet oxygen for the treatment of various skin malignancies and vascular stimulation.

2. Numerical model

2.1. Skin and brain tissue models

Heat generation is determined by the optical properties of the tissue and laser parameters such as irradiance, irradiation time, and absorption and scattering coefficients. These coefficients depend on the laser wavelength. Heat transport is solely characterized by the thermal properties of the tissue such as heat conductivity and heat capacity. In addition, the effects of heat depend on the type of tissue and the temperature reached inside it. In this study, the bioheat equation

and related boundary conditions were numerically simulated using a COMSOL Multiphysics software (COMSOL Inc., Burlington, USA). The numerical solution relies on the Finite Element Method (FEM), in which the geometry studied is divided into a finite element mesh [30]. One of the main motivations in applying the FEM for solving light propagation problems is the ability to use arbitrary geometries.

The temperature distribution in biological tissues (skin and brain) was calculated using the heat transfer module by combining the Beer-Lambert law with the Pennes bioheat transfer equation (BHTE). Previously, this model and its various modifications were used to describe laser ablation in the treatment of tumors using continuous wave (CW) [31] and pulsed lasers [32], the use of laser radiation in dermatology [33], the effects of thermal stimulation of muscles [34], skin [35] and breast tissues [36], possible heating in optogenetic neuromodulation [37], etc. The BHTE is a continuum model of vascularised tissue [38]. The influence of blood is considered as an isotropic heat source, depending on the rate of blood flow and the difference between body temperature and local tissue temperature. In fact, this model is a classical thermal equation that takes into account the influence of blood flow and metabolic heat on the energy balance in the tissue. It is assumed that the production of metabolic heat considered in this model is evenly distributed throughout the tissue. The blood perfusion is also supposed to be homogeneous and isotropic.

$$\rho C_p \frac{\partial_T}{\partial_t} = \nabla \cdot (k\nabla) + Q_{bio} + Q_{laser}, \tag{1}$$

where ρ is the density (kg/cm^3); C_p is the heat capacity (J/kg · K); k is the thermal conductivity (W/m·K); T is the temperature of the tissue (K); t is the irradiation time (s); Q_{bio} is the perfusion and metabolic heat source (W/m^3); Q_{laser} is the energy absorption of the laser irradiation (W/m^3).

$$Q_{bio} = \rho_b C_{p_b} \omega_b (T_b - T) + Q_{met}, \tag{2}$$

where p_b is the blood density (kg/cm^3); C_{p_b} is specific blood heat (J/kg ·K); ω_b is the blood perfusion rate (1/s); T_b is the arterial blood temperature (K); Q_{met} is the metabolic heat generation (W/m^3).

The laser beam intensity is determined using the Beer-Lambert Law. As the beam is absorbed, it deposits energy which acts as a heat source. Optical scattering in the biological tissue in the selected wavelength range predominates over absorption, and therefore the effective attenuation coefficient (μ_{eff}) was used based on a diffusion approximation [39].

$$Q_{laser} = \mu_a I_0 e^{-\mu_{eff} \cdot z}, \tag{3}$$

where μ_a is the absorption coefficient of the tissue (1/cm); I_0 is the irradiation intensity at the tissue surface (W/m^2); z is the depth of tissue.

$$\mu_{eff} = \sqrt{3\mu_a(\mu_a + \mu_s')}, \tag{4}$$

where μ_s' is the reduced scattering coefficient (1/cm).

2.2. Coverslip cell chamber model

In this case, the temperature distribution is calculated by combining the Beer-Lambert law (Eq. (3)) with a simple Heat transfer equation:

$$\rho C_p \frac{\partial_T}{\partial_t} = \nabla \cdot (k\nabla) + Q_{laser}. \tag{5}$$

2.3. Model parameters

To assess the temperature distribution, a one-layer brain model and a three-layer skin model are used. Table 1 gives the layer thicknesses and thermal and optical properties used in this study. These parameters were taken from the previous studies. Water parameters are temperature-dependent density, heat capacity and thermal conductivity.

Table 1. Thermal and optical properties for modeling of laser-media interaction [40–46].

Parameters	Brain	Epidermis	Dermis	Subcutaneous tissue	Water
Thickness d, mm	5	0.1	2	6	2
Density ρ, kg/m^3	1050	1200	1090	1210	$f(x)$
Heat capacity C_p, J/kg·K	3636	3950	3350	2240	$f(x)$
Thermal conductivity k, W/m·K	0.51	0.24	0.42	0.194	$f(x)$
Surface emissivity, ε	0.8	0.95	–	–	0.95
Initial temperature T, K	310.15	310.15	310.15	310.15	295.15
Arterial blood temperature T_b, K	310.15	–	310.15	310.15	–
Blood density ρ_b, kg/m^3	1035	–	1035	1035	–
Specific blood heat C_{p_b}, J/kg·K	3650	–	3650	3650	–
Blood perfusion rate ω_b, 1/s	0.01	–	0.002	0.002	–
Metabolic heat source Q_{met}, W/m^3	368	368	368	368	–
Absorption coefficient μ_a, 1/cm					
760 nm	0.74	2	1.5	1.5	0.025
1064 nm	0.76	0.3	0.7	1	0.12
1267 nm	0.78	0.8	1.2	2	0.89
Reduced scattering coefficient μ_s', 1/cm					
760 nm	64.7	39.8	25.0	21.7	–
1064 nm	45.4	28.7	17.2	16.7	–
1267 nm	37.9	25.1	14.8	15.0	–

The optical properties of skin layers and brain are considered to be a functional dependence on wavelength, and for each of the layers they were obtained from a number of sources [40–42]. The properties of water were used as thermal and optical characteristics of CCM. The effective attenuation of water is formed by the absorption coefficient when the scattering coefficient in the NIR region tends to zero [22]. Information from the COMSOL libraries [46] and a number of sources [43–45] were used to determine the thermal properties of the models. Typical values for the blood perfusion are 55 ml/min per 100g of brain tissue and 10 ml/min per 100 g of skin [47,48]. This approximately corresponds to a volumetric perfusion rate of 0.01 1/s and 0.002 1/s, respectively.

A cylinder (skin and brain tissue domains) with a radius of 5 mm and a thickness, shown in the Table 1, and a standard coverslip cell chamber with 2 mm of water are subjected to CW laser heating. For modeling, the domains are meshed using a triangle swept mesh. The laser radiation power varies from 50 to 250 mW with a step of 50 mW. The laser beam is modeled as a heat source in the plane with Gaussian profile with $\sigma = 1.7$ mm. It was supposed that the laser irradiates the tissue perpendicularly. The exposure time is 10 min. The calculations were carried out for the following wavelengths: 760 nm, 1064 nm and 1267 nm. The initial temperature was assumed to be uniform at 37 °C (310.15 K) for tissues and 22 °C (295.15 K) for water.

It is worth noting a few points. The selected power values are in the range of values used by both our and other scientific groups when studying the effect of singlet oxygen. It has been shown that similar ranges of irradiation power and time can be used both to initiate apoptosis of

cancer cells [18] and to increase the bioenergetics of cells [20]. A simplified model of biological tissues was used in our study. We assume that the surface of the brain tissue and especially the skin has a flat shape on the scale of the size of the laser beam, and in this case the heating can be described by the proposed geometry. In our study, we have not differentiated the brain tissue into the white and gray matter. Previous studies have shown that the optical characteristics of gray and white matter are almost identical in the NIR range [49,50].

3. Results

In this study, the effects of laser wavelength, exposure time, and laser power on the temperature distributions in the biological tissue are systematically examined. Figure 2(a)-c show the heat distribution during the simulation in the skin volume and surface temperature distribution for three wavelengths at a laser power of 250 mW after 10 min laser irradiation. Figure 2(d)-f and Fig. 2(g)-i demonstrate the dependence of temperature on depth and time, respectively. The distribution of laser radiation (fluence rate or irradiance for normally incident light) in the skin volume corresponding to the thermal field is presented in the Supplemental Document (see Fig. S1).
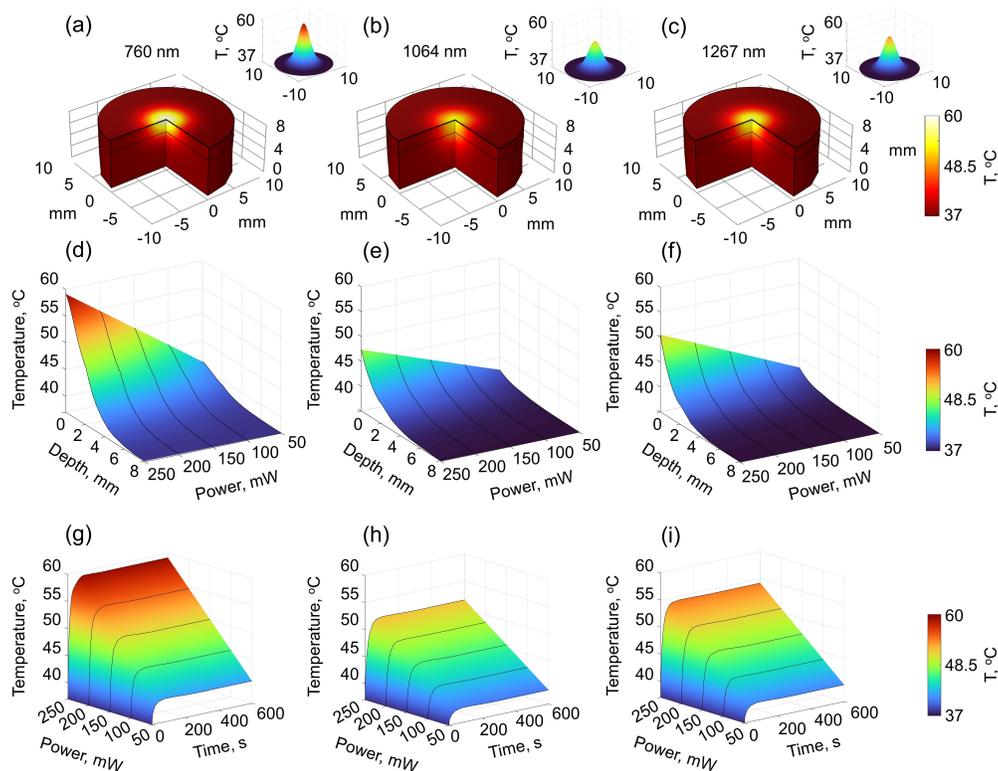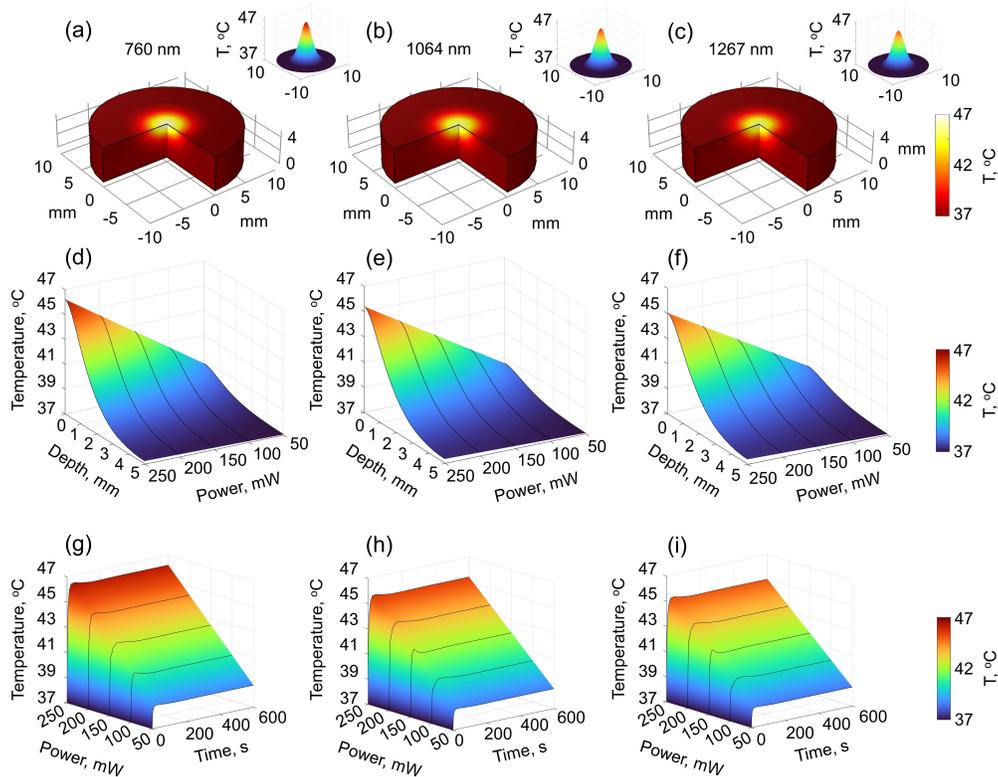

Fig. 2. Temperature distribution in the skin volume after (a) 760 nm, (b) 1064 nm and (c) 1267 nm laser irradiation with power of 250 mW during 10 min (the cones show the temperature distribution on the surface); (d-f) quantitative depth-wise temperature distribution along the skin tissue depending on the power of radiation and (g-i) temperature change on the skin surface depending on the time and power.

Due to higher absorption and scattering at a wavelength of 760 nm and a power of 250 mW, heating on the skin surface reaches 59.1 °C in 10 min. A linear change in power leads to a linear change in temperature. The results show that, for 760 nm, every 50 mW of radiation increases

the temperature by about 4.5 °C, for 1064 nm by 3.0 °C, for 1267 nm by 3.5 °C. As it can be seen in Fig. 2(d)-f, there is no significant heating in the skin at a depth of 4-5 mm. Thus, the greatest heating occurs in the epidermis and dermis. Figure 2(g)-i demonstrate temperature changes in the irradiation center on the skin surface with elapsed time. It can be seen from all graphs that the temperature rapidly increases in the early stage. The laser heating speed and power differ at different wavelengths. The laser with a wavelength of 760 nm and laser power of 250 mW provides the highest speed of heating. It is worthwhile noticing that small oscillations occur in the temperature response at the beginning of heating. This phenomenon is more obvious near the tissue surface, and it occurs due to the thermal propagation wave induced by instantaneous heating.

These measurements are consistent with the experimental temperature data collected on the skin surface using a thermal imager Testo 875 (Lenzkirch, Germany). The results of the experimental measurements are presented in the Supplemental Document (see Figs. S3a, S4a).

Figure 3(a)-c show the heat distribution in the brain tissue. Figure 3(d)-f and Fig. 3(g)-i also demonstrate the dependence of temperature on time and depth, respectively.
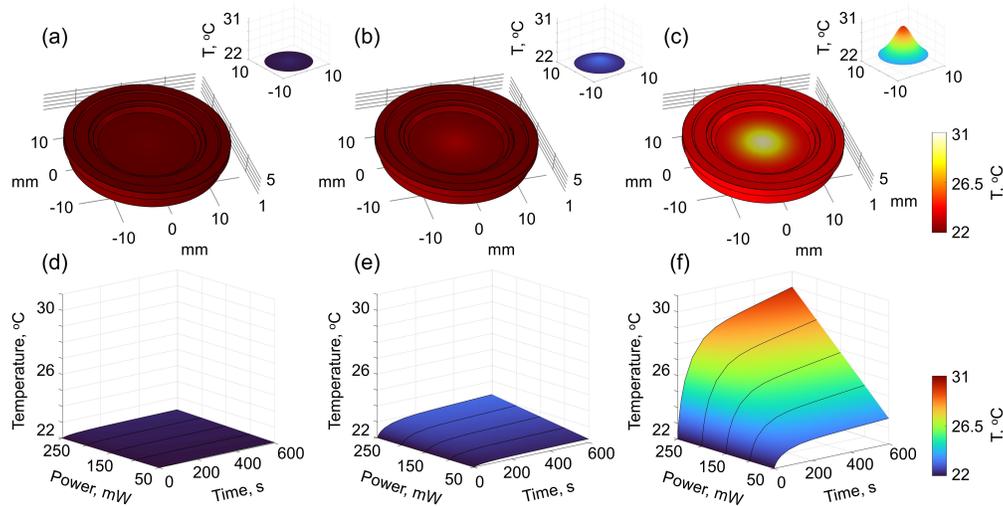

Fig. 3. Temperature distribution in the brain volume after (a) 760nm, (b) 1064 nm and (c) 1267 nm laser irradiation with power of 250 mW during 10 min (the cones show the temperature distribution on the surface); (d-f) quantitative depth-wise temperature distribution along the brain tissue depending on the power of radiation and (g-i) temperature change on the brain tissue surface depending on the time and power.

In general, for brain tissues, a heating profile similar to the skin is observed. In the early stage, the temperature rapidly increases with small oscillations. Heating on the brain surface for 760 nm can reach 46.2 °C in 10 min. The results show that for 760 nm, every 50 mW of radiation increases the temperature by about 1.9 °C, for 1064 nm by 1.7 °C, for 1267 nm by 1.6 °C. The

main differences in the heating of brain and skin tissues are caused by different absorption of chromophores (blood, water, fat) and the background. The distribution of laser radiation in the brain tissue volume corresponding to the thermal field is presented in the Supplemental Document (see Fig. S2).

Finally, we studied the heating of water in a special coverslip cell chamber for cell research. Figure 4(a)-c shows the heat distribution in the coverslip cell chamber volume for three wavelengths at a laser power of 250 mW. Figure 4(d)-f demonstrates how the coverslip surface temperature varies with time.

Fig. 4. Temperature distribution in the water after (a) 760nm, (b) 1064 nm and (c) 1267 nm laser irradiation with power of 250 mW during 10 min (the cones show the temperature distribution on the surface). (d-f) Temperature change on the coverslip surface depending on the time and power of radiation.

Here, the temperature rapidly increases in the early stage, then gradually rises, and finally approaches a steady-state value. The maximum heating of the coverslip surface reaches 30.1 °C at 1267 nm. The results show that for 760 nm, every 50 mW of radiation increases the temperature by about 0.05 °C, for 1064 nm by 0.23 °C, for 1267 nm by 1.6 °C. Such a large difference in heating is due to an order of magnitude difference in the water absorption coefficient at 1267 nm, compared to the other two wavelengths. These measurements are consistent with the experimental measurements of the temperature on the water surface in the coverslip cell chamber using a thermal imager. The experimental measurements are presented in the Supplemental Document (see Figs. S3b, S4b).

It is worth noting that the heating of the tissue is very sensitive to changes in the perfusion ω_b. A decrease in this parameter can lead to an additional significant increase in temperature. This should be taken into account when working with tissue slices and *ex vivo* samples.

4. Discussion

The simulation results obtained in this work are of great value in the context of the significant influence exerted by temperature on the chemical and biochemical reactions in living organisms.

Thermal exposure can cause either reversible tissue changes (e.g., increase of cellular metabolism, perfusion and oxygenation) at a temperature of 40-45 °C, or irreversible destruction with protein denaturation (more than 50 °C). Such tissue changes usually depend on both time and

temperature and can affect perfusion, as well as the mechanical, electrical and thermal properties of tissues.

Heat increases kinetic energy in cells by speeding up the molecules involved in chemical reactions. In general, the effect of temperature on the rate of biological processes can be described using the Arrhenius equation. At the same time, this effect can be a more complex and multistep process, such as aerobic metabolism, that relies on mechanisms acting across multiple levels of biological organization [51].

Aerobic metabolism, which plays an important role in providing the energy necessary for the life of the body, is characterized by high sensitivity to temperature rise. As demonstrated in [52], the reactions of aerobic metabolism and their speed directly depend on the surrounding temperature. According to the oxygen and capacity limited thermal tolerance hypothesis, the temperature changes towards low and high values exceeding the thermal optimum of thermal performance curve [53] can lead to a decrease in oxygen levels in body fluids. At high temperatures, this decrease reflects an excessive need for oxygen. At the same time, when high critical temperatures are reached as a result of the transition to anaerobic mitochondrial metabolism, the complete disappearance of the aerobic scope can be observed [54].

The high temperature can also lead to a change in the fluidity of the membranes [55]. These changes in membrane fluidity can have direct effects on the activity of membrane-embedded proteins [56]. The increase in membrane fluidity activates the flow of protons through the inner membrane of mitochondria along pathways other than ATP synthase, thereby reducing the efficiency of mitochondrial ATP production [57]. The paper [58] notes that exposure to high temperature can lead to disruption of lipid-protein interactions, which in turn can cause a violation of mitochondrial respiration. Considering the potentially dangerous side effects of mitochondrial respiration in connection with reactive oxygen species production, the analysis of tissue heating is important. This can be attributed to the fact that the production of ROS by mitochondria increases with temperature [59,60], thereby contributing to the damage of cellular macromolecules (lipids, proteins and DNA) and to the violation of the structure and function of cells and tissues. Thus, temperature control is an essential part of the study of processes in living objects.

In addition, the importance of analyzing the possible heating at the selected parameters of laser exposure increases, taking into account the organization of living objects and the complex interdependencies of aerobic metabolism. For complex living systems, it becomes difficult to determine the exact level of biological organization at which a violation occurs, leading to a deterioration of metabolism and, consequently, factors of regulation of organs and systems [51].

The above demonstrates the importance of taking temperature into account when conducting experimental studies at the cellular and organismal levels. Although modern methods of thermal imaging can register temperature changes on the surface of an object with high sensitivity, they do not allow estimating the distribution of heat over depth, as well as predicting the effect of temperature. Computer modeling is preferred in this case.

The results of the study show that, for direct optical generation of singlet oxygen, it is reasonable to increase the dose by increasing the exposure time while reducing the radiation power. At the same time, pulsed lasers can be particularly helpful in reducing thermal loads. It was previously shown that the PDT efficiency using a pulsed laser may be identical to the CW laser with the same wavelength [61]. In addition, the use of pulsed lasers makes it possible to develop effective singlet oxygen detection systems based on the registration of the luminescence lifetime [62]. The use of control lasers with equivalent values of the effective attenuation coefficient makes it possible to perform a comparative analysis. This knowledge should be taken into account when conducting research related to the study of the effect of laser-induced singlet oxygen on the bioenergetics of cancer cells [18], neurons [20], vascular tone [63], etc.

Finally, the results obtained can be useful not only in the field of singlet oxygen generation, but also in various applications of optogenetics, optical tweezers, laser surgery, Raman spectroscopy, etc.

5. Conclusion

In this work, *in silico* studies were performed to investigate how optical radiation of various wavelengths for the direct optical generation of singlet oxygen interacts with biological tissues, causing them to heat up. Temperature distribution along multiple skin layers, brain tissue and cell culture media was analysed using a numerical solution of the bioheat equation in the finite element solver, COMSOL Multiphysics software. The developed model allows to predict the optimal parameters of the experimental singlet oxygen generation system excluding the heating of biological tissues and cell cultures. The present findings could also be considered in order for the specialists to accurately specify the laser optical dose in various biomedical applications.

Although some inaccuracies of the simulation may be caused by the input thermal and optical properties, which vary in different studies, the model shows good agreement with experimental data.

Disclosures. The authors declare that there are no conflicts of interest related to this article.

Data availability. Data underlying the results may be obtained from the authors upon reasonable request.

Supplemental document. See Supplement 1 for supporting content.

References

1. W. A. Pryor, K. N. Houk, C. S. Foote, J. M. Fukuto, L. J. Ignarro, G. L. Squadrito, and K. J. A. Davies, "Free radical biology and medicine: it's a gas, man!" Am. J. Physiol. Regul. Integr. Comp. Physiol. **291**(3), R491–R511 (2006).
2. W. Dröge, "Free radicals in the physiological control of cell function," Physiol. Rev. **82**(1), 47–95 (2002).
3. C. Bergamini, S. Gambetti, A. Dondi, and C. Cervellati, "Oxygen, Reactive Oxygen Species and Tissue Damage," Curr. Pharm. Des. **10**(14), 1611–1626 (2004).
4. D. R. Kearns, "Physical and chemical properties of singlet molecular oxygen," Chem. Rev. **71**(4), 395–427 (1971).
5. T. Devasagayam and J. P. Kamat, "Biological significance of singlet oxygen," Indian J. Exp. Biol. **40**(6), 680–692 (2002).
6. P. D. Mascio, G. R. Martinez, S. Miyamoto, G. E. Ronsein, M. H. G. Medeiros, and J. Cadet, "Singlet Molecular Oxygen Reactions with Nucleic Acids, Lipids, and Proteins," Chem. Rev. **119**(3), 2043–2086 (2019).
7. C. Schweitzer and R. Schmidt, "Physical mechanisms of generation and deactivation of singlet oxygen," Chem. Rev. **103**(5), 1685–1758 (2003).
8. M. Niedre, M. S. Patterson, and B. C. Wilson, "Direct near-infrared luminescence detection of singlet oxygen generated by photodynamic therapy in cells *in vitro* and tissues *in vivo*," Photochem. Photobiol. **75**(4), 382–391 (2002).
9. M. C. DeRosa and R. J. Crutchley, "Photosensitized singlet oxygen and its applications," Coord. Chem. Rev. **233-234**, 351–371 (2002).
10. R. D. Almeida, B. J. Manadas, A. P. Carvalho, and C. B. Duarte, "Intracellular signaling mechanisms in photodynamic therapy," Biochim. Biophys. Acta, Rev. Cancer **1704**(2), 59–86 (2004).
11. F. Anquez, A. Sivéry, I. El Yazidi-Belkoura, J. Zemmouri, P. Suret, S. Randoux, and E. Courtade, "Chapter 4 production of singlet oxygen by direct photoactivation of molecular oxygen," in *Singlet Oxygen: Applications in Biosciences and Nanosciences, Volume 1*, vol. 1 (Royal Society of Chemistry, 2016), pp. 75–91.
12. T. Aabo, I. R. Perch-Nielsen, J. S. Dam, D. Z. Palima, H. Siegumfeldt, J. Glückstad, and N. Arneborg, "Effect of long- and short-term exposure to laser light at 1070 nm on growth of Saccharomyces cerevisiae," J. Biomed. Opt. **15**(4), 041505 (2010).

13. Z. Pilát, J. Ježek, M. Šerý, M. Trtílek, L. Nedbal, and P. Zemánek, "Optical trapping of microalgae at 735–1064nm: Photodamage assessment," J. Photochem. Photobiol., B **121**, 27–31 (2013).

14. M. R. Detty, "Direct 1270 nm irradiation as an alternative to photosensitized generation of singlet oxygen to induce cell death," Photochem. Photobiol. **88**(1), 2–4 (2012).

15. M. Bregnhøj, A. Blázquez-Castro, M. Westberg, T. Breitenbach, and P. R. Ogilby, "Direct 765 nm Optical Excitation of Molecular Oxygen in Solution and in Single Mammalian Cells," J. Phys. Chem. B **119**(17), 5422–5429 (2015).

16. A. Blázquez-Castro, "Direct $^1O_2$ optical excitation: A tool for redox biology," Redox Biol. **13**, 39–59 (2017).

17. S. G. Sokolovski, S. A. Zolotovskaya, A. Goltsov, C. Pourreyron, A. P. South, and E. U. Rafailov, "Infrared laser pulse triggers increased singlet oxygen production in tumour cells," Sci. Rep. **3**(1), 3484 (2013).

18. F. Anquez, I. El Yazidi-Belkoura, S. Randoux, P. Suret, and E. Courtade, "Cancerous cell death from sensitizer free photoactivation of singlet oxygen," Photochem. Photobiol. **88**(1), 167–174 (2012).

19. Y. Saenko, E. S. Glushchenko, I. Zolotovskii, E. M. Sholokhov, and A. S. Kurkov, "Mitochondrial dependent oxidative stress in cell culture induced by laser radiation at 1265 nm," Lasers Med. Sci. **31**(3), 405–413 (2016).

20. S. G. Sokolovski, E. U. Rafailov, A. Y. Abramov, and P. R. Angelova, "Singlet oxygen stimulates mitochondrial bioenergetics in brain cells," Free Radical Biol. Med. **163**, 306–313 (2021).

21. E. J. Peterman, F. Gittes, and C. F. Schmidt, "Laser-Induced Heating in Optical Traps," Biophys. J. **84**(2), 1308–1316 (2003).

22. G. M. Hale and M. R. Querry, "Optical constants of water in the 200-nm to 200-μm wavelength region," Appl. Opt. **12**(3), 555–563 (1973).

23. J. Sakakibara and R. J. Adrian, "Whole field measurement of temperature in water using two-color laser induced fluorescence," Exp. Fluids **26**(1-2), 7–15 (1999).

24. S. Ebert, K. Travis, B. Lincoln, and J. Guck, "Fluorescence ratio thermometry in a microfluidic dual-beam laser trap," Opt. Express **15**(23), 15493–15499 (2007).

25. F. Wetzel, S. Rönicke, K. Müller, M. Gyger, D. Rose, M. Zink, and J. Käs, "Single cell viability and impact of heating by laser absorption," Eur. Biophys. J. **40**(9), 1109–1114 (2011).

26. Y. Liu, G. Sonek, M. Berns, and B. Tromberg, "Physiological monitoring of optically trapped cells: assessing the effects of confinement by 1064-nm laser tweezers using microfluorometry," Biophys. J. **71**(4), 2158–2167 (1996).

27. K. Okabe, N. Inada, C. Gota, Y. Harada, T. Funatsu, and S. Uchiyama, "Intracellular temperature mapping with a fluorescent polymeric thermometer and fluorescence lifetime imaging microscopy," Nat. Commun. **3**(1), 705 (2012).

28. J. S. Donner, S. A. Thompson, M. P. Kreuzer, G. Baffou, and R. Quidant, "Mapping Intracellular Temperature Using Green Fluorescent," Nano Lett. **12**(4), 2107–2111 (2012).

29. F. Vetrone, R. Naccache, A. Zamarrón, A. J. d. l. Fuente, F. Sanz-Rodríguez, L. M. Maestro, E. M. Rodriguez, D. Jaque, J. G. Solé, and J. A. Capobianco, "Temperature Sensing Using Fluorescent Nanothermometers," ACS Nano **4**(6), 3254–3258 (2010).

30. N. Ottosen and H. Petersson, *Introduction to the Finite Element Method* (Prentice-Hall, 1992).

31. V. N. Tran, V. G. Truong, Y. W. Lee, and H. W. Kang, "Effect of optical energy modulation on the thermal response of biological tissue: computational and experimental validations," Biomed. Opt. Express **11**(12), 6905–6919 (2020).

32. M. Ganguly, S. Miller, and K. Mitra, "Model development and experimental validation for analyzing initial transients of irradiation of tissues during thermal therapy using short pulse lasers," Lasers Surg. Med. **47**(9), 711–722 (2015).

33. W. Shen, J. Zhang, and F. Yang, "Three-dimensional model on thermal response of skin subject to laser heating," Comput. Methods Biomech. Biomed. Eng. **8**(2), 115–125 (2005).

34. J. Kocbach, K. Folgerø, L. Mohn, and O. Brix, "A simulation approach to optimizing performance of equipment for thermostimulation of muscle tissue using comsol multiphysics," Biophysics & Bioeng. Letters **4**, 9–33 (2011).

35. K. Shurrab, N. Kochaji, and W. Bachir, "Development of temperature distribution and light propagation model in biological tissue irradiated by 980 nm laser diode and using comsol simulation," J. Lasers Med. Sci. **8**(3), 118–122 (2017).

36. Y. He, M. Shirazaki, H. Liu, R. Himeno, and Z. Sun, "A numerical coupling model to analyze the blood flow, temperature, and oxygen transport in human breast tumor under laser irradiation," Comput. Biol. Med. **36**(12), 1336–1350 (2006).

37. Y. Shin, M. Yoo, H.-S. Kim, S.-K. Nam, H.-I. Kim, S.-K. Lee, S. Kim, and H.-S. Kwon, "Characterization of fiber-optic light delivery and light-induced temperature changes in a rodent brain for precise optogenetic neuromodulation," Biomed. Opt. Express **7**(11), 4450–4471 (2016).

38. H. H. Pennes, "Analysis of tissue and arterial blood temperatures in the resting human forearm," J. Appl. Physiol. **1**(2), 93–122 (1948).

39. A. Ishimaru, "Diffusion of light in turbid material," Appl. Opt. **28**(12), 2210–2215 (1989).

40. V. Dremin, E. Zherebtsov, A. Bykov, A. Popov, A. Doronin, and I. Meglinski, "Influence of blood pulsation on diagnostic volume in pulse oximetry and photoplethysmography measurements," Appl. Opt. **58**(34), 9398–9405 (2019).

41. E. V. Salomatina, B. Jiang, J. Novak, and A. N. Yaroslavsky, "Optical properties of normal and cancerous human skin in the visible and near-infrared spectral range," J. Biomed. Opt. **11**(6), 064026 (2006).

42. E. A. Genina, A. N. Bashkatov, D. K. Tuchina, P. A. Dyachenko, N. Navolokin, A. Shirokov, A. Khorovodov, A. Terskov, M. Klimova, A. Mamedova, I. Blokhina, I. Agranovich, E. Zinchenko, O. V. Semyachkina-Glushkovskaya,

and V. V. Tuchin, "Optical properties of brain tissues at the different stages of glioma development in rats: pilot study," Biomed. Opt. Express **10**(10), 5182–5197 (2019).

43. D. A. Torvi and J. D. Dale, "A Finite Element Model of Skin Subjected to a Flash Fire," J. Biomech. Eng. **116**(3), 250–255 (1994).

44. T. R. Gowrishankar, D. A. Stewart, G. T. Martin, and J. C. Weaver, "Transport lattice models of heat transport in skin with spatially heterogeneous, temperature-dependent perfusion," Biomed. Eng. Online **3**(1), 42 (2004).

45. "IT'IS Foundation," www.itis.swiss/virtual-population/tissue-properties/database/. Accessed: 2021-11-20.

46. "COMSOL - Software for Multiphysics Simulation," www.comsol.com/. Accessed: 2021-11-20.

47. O. P. Tandon and Y. Tripathi, *Best & Taylor's: physiological basis of medical practice* (Lippincott Williams and Wilkins, 2011).

48. A. C. Guyton, *Textbook of medical physiology* (Elsevier Saunders, 2006).

49. A. N. Yaroslavsky, P. C. Schulze, I. V. Yaroslavsky, R. Schober, F. Ulrich, and H.-J. Schwarzmaier, "Optical properties of selected native and coagulated human brain tissues in vitro in the visible and near infrared spectral range," Phys. Med. Biol. **47**(12), 2059–2073 (2002).

50. N. Honda, K. Ishii, Y. Kajimoto, T. Kuroiwa, and K. Awazu, "Determination of optical properties of human brain tumor tissues from 350 to 1000 nm to investigate the cause of false negatives in fluorescence-guided resection with 5-aminolevulinic acid," J. Biomed. Opt. **23**(07), 1 (2018).

51. P. M. Schulte, J. E. Podrabsky, J. H. Stillman, and L. Tomanek, "The effects of temperature on aerobic metabolism: towards a mechanistic understanding of the responses of ectotherms to a changing environment," J. Exp. Biol. **218**(12), 1856–1866 (2015).

52. P. W. Hochachka and G. N. Somero, *Biochemical Adaptation: Mechanisms and Process in Physiology Evolution* (Oxford University Press, 2002).

53. P. M. Schulte, T. M. Healy, and N. A. Fangue, "Thermal Performance Curves, Phenotypic Plasticity, and the Time Scales of Temperature Exposure," Integr. Comp. Biol. **51**(5), 691–702 (2011).

54. H. Pörtner, "Climate change and temperature-dependent biogeography: oxygen limitation of thermal tolerance in animals," Naturwissenschaften **88**(4), 137–146 (2001).

55. J. R. Hazel, "Thermal adaptation in biological membranes: Is homeoviscous adaptation the explanation?" Annu. Rev. Physiol. **57**(1), 19–42 (1995).

56. G. N. Somero, "Temperature relationships: From molecules to biogeography," in *Comprehensive Physiology*, (John Wiley & Sons, Ltd, 2011), pp. 1391–1444.

57. F. Seebacher, M. Brand, P. Else, H. Guderley, A. Hulbert, and C. Moyes, "Plasticity of oxidative metabolism in variable climates: Molecular mechanisms," Physiol. Biochem. Zool. **83**(5), 721–732 (2010).

58. J. O'Brien, E. Dahlhoff, and G. N. Somero, "Thermal resistance of mitochondrial respiration: Hydrophobic interactions of membrane proteins may limit thermal resistance," Physiol. Zool. **64**(6), 1509–1526 (1991).

59. D. Abele, K. Heise, H. O. Pörtner, and S. Puntarulo, "Temperature-dependence of mitochondrial function and production of reactive oxygen species in the intertidal mud clam mya arenaria," J. Exp. Biol. **205**(13), 1831–1841 (2002).

60. S. Venkataraman, B. A. Wagner, X. Jiang, H. P. Wang, F. Q. Schafer, J. M. Ritchie, B. C. Patrick, L. W. Oberley, and G. R. Buettner, "Overexpression of manganese superoxide dismutase promotes the survival of prostate cancer cells exposed to hyperthermia," Free Radic. Res. **38**(10), 1119–1132 (2004).

61. D. Chen, Y. Wang, B. Li, H. Lin, X. Lin, and Y. Gu, "Effects of pulse width and repetition rate of pulsed laser on kinetics and production of singlet oxygen luminescence," J. Innov. Opt. Health Sci. **09**(06), 1650019 (2016).

62. N. R. Gemmell, A. McCarthy, B. Liu, M. G. Tanner, S. D. Dorenbos, V. Zwiller, M. S. Patterson, G. S. Buller, B. C. Wilson, and R. H. Hadfield, "Singlet oxygen luminescence detection with a fiber-coupled superconducting nanowire single-photon detector," Opt. Express **21**(4), 5005–5013 (2013).

63. H. Buzzá, L. Silva, L. Moriyama, V. Bagnato, and C. Kurachi, "Evaluation of vascular effect of photodynamic therapy in chorioallantoic membrane using different photosensitizers," J. Photochem. Photobiol., B **138**, 1–7 (2014).